THE JOURNAL OF PHYSICAL CHEMISTRY A

ARTICLE

pubs.acs.org/JPCA

Femtosecond Transient Absorption Spectroscopic Study of a Carbonyl-Containing Carotenoid Analogue, 2-(all-*trans*-Retinylidene)-indan-1,3-dione

Toshiyuki Kusumoto,[†] Daisuke Kosumi,[†] Chiasa Uragami,[†] Harry A. Frank,[‡] Robert R. Birge,[‡] Richard J. Cogdell,[§] and Hideki Hashimoto*[,†,∥]

[†]CREST/JST and Department of Physics, Graduated School of Science, Osaka City University, 3-3-138 Sugimoto, Sumiyoshi-ku, Osaka 558-8585, Japan

[‡]Department of Chemistry, University of Connecticut, 55 North Eagleville Road, Storrs, Connecticut 06269-3060, United States

[§]Institute for Molecular, Cell and Systems Biology, Glasgow Biomedical Research Centre, University of Glasgow, 120 University Place, Glasgow G12 8QQ, Scotland, United Kingdom

[∥]The Osaka City University Advanced Research Institute for Natural Science and Technology (OCARINA), 3-3-138 Sugimoto, Sumiyoshi-ku, Osaka 558-8585, Japan

ABSTRACT: The photophysical properties of a carbonyl-containing carotenoid analogue in an *s-cis* configuration, relative to the conjugated π system, 2-(all-*trans*-retinylidene)-indan-1,3-dione (C20Ind), were investigated by femtosecond time-resolved spectroscopy in various solvents. The lifetime of the optically forbidden S_1 state of C20Ind becomes long as solvent polarity increases. This trend is completely opposite to the situation of $S_{1\text{-ICT}}$ dynamics of carbonyl-containing carotenoids, such as peridinin and fucoxanthin. Excitation energy dependence of the transient absorption measurements shows that the transient absorption spectra in nonpolar solvents were originated from two distinct transient species, while those in polar and protic solvents are due to a single transient species. By referring to the results of MNDO-PSDCI (modified neglect of differential overlap with partial single- and double-configuration interaction) calculations, we conclude: (1) in polar and protic solvents, the S_1 state is generated following excitation up to the S_2 state; (2) in nonpolar solvents, however, both the S_1 and the $^1n\pi^*$ states are generated; and (3) C20Ind does not generate the $S_{1\text{-ICT}}$ state, despite the fact that it has two conjugated carbonyl groups.

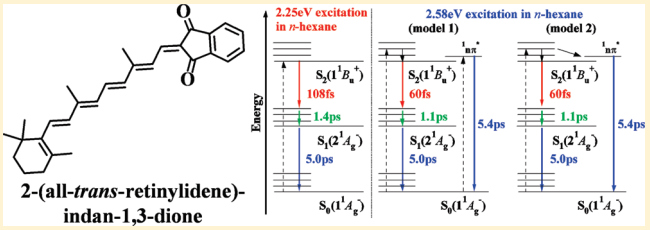

INTRODUCTION

Carotenoids are naturally occurring chromophores containing a long-chain polyene backbone and play an important role in photosynthesis acting as accessory light harvesting molecules.[1,2] The singlet excited states of carotenoids without carbonyls are designated by referring to an idealized C_{2h} point symmetry group.[2,3] The lowest optically allowed singlet excited state is the $1^1B_u^+$ state (S_2), and an optically forbidden $2^1A_g^-$ state (S_1) exists below S_2. The presence of an intramolecular charge transfer (S_{ICT}) state coupled to the S_1 state ($S_{1\text{-ICT}}$) have been reported for carbonyl-containing carotenoids, such as peridinin, in solution and in pigment−protein complexes.[4−9] The $S_{1\text{-ICT}}$ state plays a key role in the photophysical properties of carbonyl-containing carotenoids as was shown by transient absorption spectroscopic measurements.[10−13] The lifetime of the S_1 was found to become shorter as the length of the π-conjugation increases[10−13] similar to the behavior of carotenoids without carbonyls.[14,15] In contrast, the $S_{1\text{-ICT}}$ state lifetimes are invariant with respect to the conjugated chain length.[10−13] These experimental findings are supported by quantum-chemical calculations.[16−18] Models of the $S_{1\text{-ICT}}$ state have been proposed on the basis of evolution of the S_1 state.[4−13,16−18] Recently, it was reported that the S_1 and S_{ICT} states of fucoxanthin can be generated distinctly by selecting two-photon excitation.[19] The situation of peridinin, however, is more complicated, and a distinction of S_1 and $S_{1\text{-ICT}}$ is not straightforward.[9] In the case of 3′-hydroxyechinenone (heCN), its $S_{1\text{-ICT}}$ state was not found to be generated in solution, but it is formed in the orange carotenoid protein (OCP) from the cyanobacterium *Arthrospira maxima*.[20] The carbonyl group of heCN in OCP is locked in an *s-trans* configuration to its polyene backbone.[20] Furthermore, canthaxanthin and rhodoxanthin with terminal ring structures containing carbonyl groups do not produce an $S_{1\text{-ICT}}$ state in solution because of the twisted geometry of the terminal rings with respect to the conjugated polyene backbone.[21] These phenomena suggest that the conformation of a carbonyl group to the π-conjugated system in polyene backbone plays an important role in the generation of the $S_{1\text{-ICT}}$ state.

Received: November 29, 2010
Revised: January 27, 2011
Published: March 01, 2011

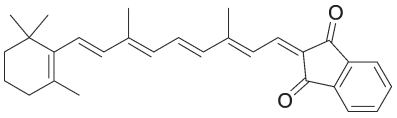

Figure 1. Chemical structure of 2-(all-*trans*-retinylidene)-indan-1,3-dione (C20Ind).

Moreover, there is another excited singlet state that complicates the photophysics of these polyenes. The presence of a low-lying $^1n\pi^*$ state is a general feature of polyenes with a carbonyl group, such as benzophenone, *trans*-β-hydrindanone, and linear polyenals.[22−24] This state plays important role in intersystem crossing from the singlet to triplet state as well as the trans to cis isomerization.[22,25] The presence of the $^1n\pi^*$ state between the S_1 and ground state (S_0) was reported in retinal having five conjugated double bonds and an aldehyde-type carbonyl group.[26−29] The lifetime of the $^1n\pi^*$ state of retinal in protic solvents is shorter than that in nonpolar solvents.[29] However, as yet there is no clear evidence for the presence of the $^1n\pi^*$ state in carotenoids with carbonyl groups except for the case of siphonaxanthin.[30]

In a previous study, we synthesized a carotenoid analogue with two carbonyl groups, 2-(all-*trans*-retinylidene)-indan-1,3-dione (abbreviated as C20Ind, see Figure 1 for chemical structure).[31] The conjugation of C20Ind extended onto both the carbonyls but not onto the indan ring. It has six carbon−carbon conjugated double bonds attached onto a branched double bond.[31] This conjugation pattern is very similar to that of peridinin. The structure of C20Ind has been determined by X-ray crystallography.[31] The carbonyl groups of C20Ind were locked in the *s-cis* conformation in relation to the conjugated polyene chain. This suggests that C20Ind represents a simplified model to help examine the role of the carbonyl group in the generation of the $S_{1\text{-ICT}}$ and/or $^1n\pi^*$ states.

The aim of this present study is to investigate the formation of the $S_{1\text{-ICT}}$ and/or $^1n\pi^*$ states in a short carotenoid with two carbonyl groups in an *s-cis* conformation. We present here a combined experimental and theoretical study of C20Ind. Our experimental methods include electronic and Raman spectroscopy as well as femtosecond time-resolved absorption spectroscopy in a variety of solvents. Our theoretical method is MNDO-PSDCI (modified neglect of differential overlap with partial single- and double-configuration interaction) theory including full single and double configuration interaction (CI) within the π system.

EXPERIMENTAL METHODS

Sample Preparation and Solvents Used in This Study. C20Ind was synthesized and purified as previously reported.[31] Retinyl acetate was purchased from BASF (Switzerland) and purified by silica gel column chromatography and subsequent recrystallization from *n*-hexane. Indan-1,3-dione was purchased from Tokyo Kasei (Japan) and used as received. The all-*trans* retinal was prepared by the hydrolysis of retinyl acetate followed by oxidation using MnO_2 (Aldrich Chemicals, U.S.). C20Ind was prepared by means of a modified Knoevenagel condensation of retinal and indan-1,3-dione in methanol.

C20Ind was dissolved in nonpolar, *n*-hexane (Kishida Chemical, Japan) and toluene (WAKO Chemical, Japan), in polar, THF (WAKO Chemical, Japan), acetone (Kishida Chemical, Japan), and acetonitrile (Kishida Chemical, Japan), and in protic, methanol (Kishida Chemical, Japan), solvents for the following studies.

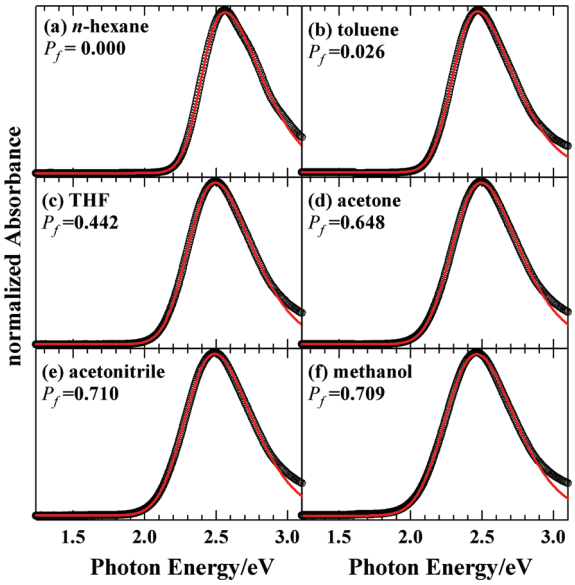

Figure 2. Steady-state absorption spectra of C20Ind in (a) *n*-hexane, (b) toluene, (c) THF, (d) acetone, (e) acetonitrile, and (f) methanol. P_f is the solvent polarity factor, which was determined from the dielectric constant ε and the refractive index n of the solvents using the expression, $P_f = (\varepsilon - 1)/(\varepsilon + 2) - (n^2 - 1)/(n^2 + 2)$. Circles indicate the experimental data. Solid lines indicate the results of spectral fitting based on a Franck−Condon analysis. All the spectra are normalized at the absorption maximum.

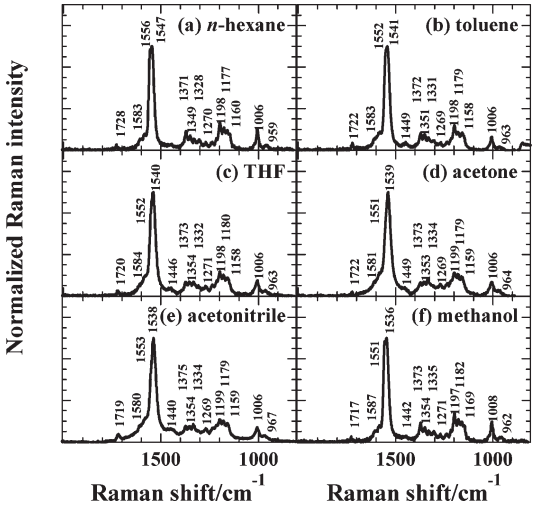

Figure 3. Spontaneous resonance Raman spectra of C20Ind in (a) *n*-hexane, (b) toluene, (c) THF, (d) acetone, (e) acetonitrile, and (f) methanol observed at 532 nm excitation. Raman lines due to solvents are subtracted. All the spectra are normalized at the highest peak signals.

Steady-State Absorption and Resonance Raman Spectroscopic Measurements. The optical density of C20Ind was adjusted to 1 at the maximum of the steady-state absorption spectrum. The steady-state absorption spectra were measured using a conventional spectrophotometer (V-670, Jasco, Japan). A diode-pumped solid-state CW-laser with output at 532 nm (SDL-532-SLM-030T, Shanghai Dream Lasers Technology, China) was used as the excitation light-source to generate resonance Raman spectra of C20Ind. The Raman scattering

Table 1. Huang−Rhys Factor, 0−0 Transition Energy, Vibrational Energy of the C=C Stretching Mode, and a Full Width at Half-Maximum (fwhm) Determined by Franck−Condon Analysis of the Steady-State Absorption Spectra of C20Ind in Various Solvents

	n-hexane	toluene	THF	acetone	acetonitrile	methanol
Huang−Rhys factor	1.401	1.368	1.404	1.393	1.377	1.357
0−0 transition energy/eV	2.487	2.385	2.395	2.388	2.381	2.347
vibrational energy/eV	0.1928	0.1918	0.1919	0.1908	0.1907	0.1905
fwhm/eV	0.2004	0.2155	0.2412	0.2602	0.2688	0.2899

was detected by using a liquid nitrogen cooled CCD camera (LN/CCD-576-E/1, Roper Scientific, Japan) attached to a spectrometer (U1000, Horiba-Jovin-Ybon, Japan). The back-scattering optical geometry was used, and all measurements were performed at room temperature.

Femtosecond Transient Absorption Spectroscopic Measurements. The absorbance of C20Ind was adjusted to 0.5 at the maximum of steady-state absorption spectra in 1 mm optical path-length quartz cell. The experimental setup of the femtosecond transient absorption measurements was as described in a previous paper.[32] A mode-locked Ti:Sapphire oscillator and a 1 kHz regenerative amplifier (Hurricane-X, Spectra Physics, U.S.) provided the excitation and probe pulses. Excitation pulses were obtained by sum-frequency mixing the output of an optical parametric amplifier (OPA-800CF, Spectra Physics, U.S.) with a residual fundamental pulse in a 1.0 mm BBO crystal. The excitation energy was adjusted to 20 nJ/pulse. A white light continuum probe pulse, generated using a 5.0 mm sapphire plate, was detected by a photodiode array (1024 pixels NMOS linear image sensor S3903-1024G, Hamamatsu, Japan) through a spectrometer (Acton SP275i, Princeton Instruments, U.S.). The excitation pulses were modulated at 500 Hz by an optical chopper (C-995 Optical Chopper, Terahertz Technologies Inc., U.S.), and the data output was synchronized with the laser repetition of 1 kHz using home-built electronic circuitry.[32]

The instrumental response function of the system determined by cross-correlation between the excitation and probe pulses was better than 100 fs. The cross-correlation function was used to determine the zero time delay at each probe energy. After chirp compensation, the uncertainty in the zero time delay was less than 20 fs.

Quantum-Chemical Calculation. The ground-state equilibrium geometry and ground-state properties of C20Ind were calculated by using Gaussian 03, the B3LYP density functional, and a 6-31G(d) basis set.[33] The excited-state electronic properties were calculated by using MNDO-PSDCI molecular orbital theory and an AM1 Hamiltonian. Quantum-chemical calculations using MNDO-PSDCI, SAC-CI, and TDDFT methods have been applied to a carbonyl containing carotenoid fucoxanthin.[18] None of each calculation can fully explain the properties of the S_{ICT} state of fucoxanthin, but some parts of the experimental results were satisfactorily interpreted using the results of these calculations. Among these three calculation methods, SAC-CI is the highest end, but it needs sufficiently high computer resource and huge amount of calculation time for the practical usage. Nevertheless, calculations using this method cannot correctly predict the values of parameter $|\Delta\mu|$ (change of static dipole moment of molecules upon photoexcitation) that is important to discuss the property of S_{ICT}. The TDDFT method is useful to theoretically predict $|\Delta\mu|$ values, but it does not correctly predict the ordering of the singlet excited states of fucoxanthin. The MNDO-PSDCI method is handy to use and can correctly reproduce the ordering of the S_1 ($2^1A_g^-$), S_2 ($1^1B_u^-$), and S_3 ($1^1B_u^+$) states as can be done using the SAC-CI method. Therefore, we have adopted the MNDO-PSDCI method in this present study. MNDO-PSDCI calculations using an AM1 Hamiltonian were applied to C20Ind whose structure was optimized in the S_0 ground state using DFT method. These methods have been applied successfully to the study of several comparable systems including carbonyl-containing carotenoids.[17,18,34−43] We carried out full single and double CI calculations within the eight highest energy filled π orbitals, the eight lowest energy unfilled π orbitals, and the two highest energy filled n orbitals. The MNDO-PSDCI programs are available by contacting R. R. Birge (rbirge@uconn.edu).

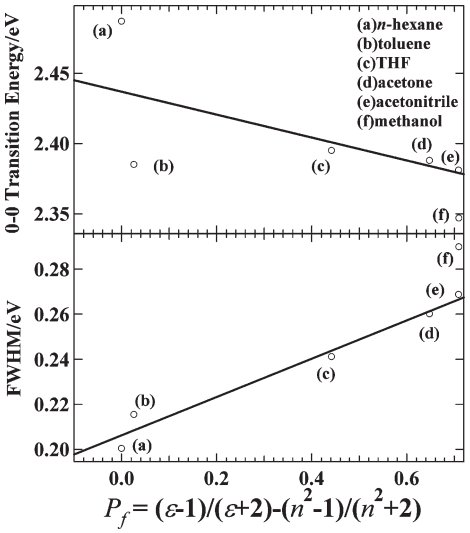

Figure 4. Solvent polarity dependences of the 0−0 transition energy (top) and a full width at half-maximum (fwhm) (bottom) of the absorption bands of C20Ind. The "○" show the experimental results. Solid lines show the results of the least-squares fittings except for the data points in methanol ((f) in this figure).

RESULTS AND DISCUSSION

Steady-State Absorption and Resonance Raman Spectra. Figure 2 shows steady-state absorption spectra of C20Ind in several solvents. In all cases, the vibronic development of the $S_0 \rightarrow S_2$ transition cannot be resolved due to inhomogeneous broadening. However, it is clearly seen that the energy of the maximum absorbance is red-shifted when increasing solvent polarity. This red shift is caused by an electrostatic solvent effect as has already been observed in other carbonyl-containing carotenoids.[4,5,10−13] Figure 3 shows resonance Raman spectra of C20Ind in the same set of solvents. On the basis of the assignment of the Raman bands in previous papers, the Raman lines observed for C20Ind can be empirically assigned as below.[44−49] The Raman lines in the 959−967 spectral region are assigned to the C−C−H out-of-plane bending vibration.

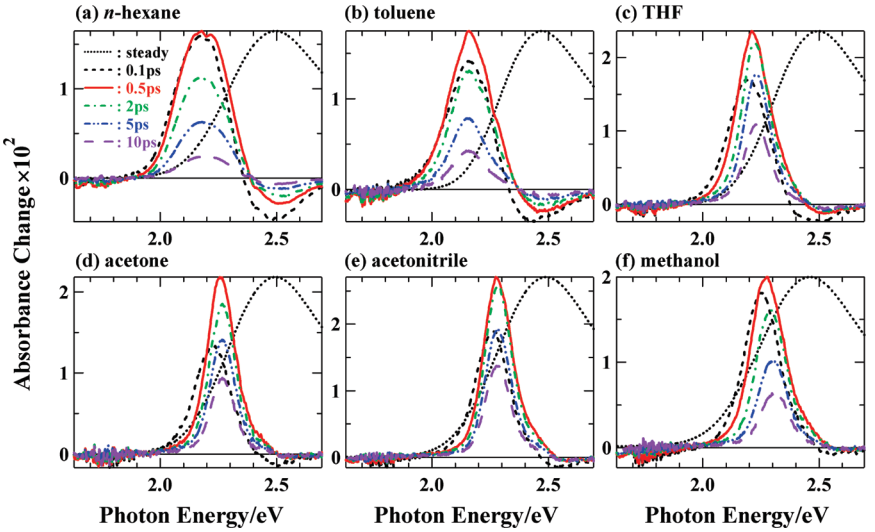

Figure 5. Femtosecond transient absorption spectra of C20Ind following excitation at 2.43 eV in (a) *n*-hexane, (b) toluene, (c) THF, (d) acetone, (e) acetonitrile, and (f) methanol. Dotted lines show the steady-state absorption spectra. Dashed, solid, dashed−dotted, dashed double-dotted, and long-dashed lines show the femtosecond transient absorption spectra recorded at 0.1, 0.5, 2.0, 5.0, and 10 ps after excitation, respectively.

Those around 1007 cm^{-1} are assigned to methyl in-plane rocking vibrations. Those around 1270 cm^{-1} are assigned to the coupling mode between C−C−H bendings and the carbon−carbon single and double bond stretching vibrations. Those in the 1200−1150 and 1550−1530 cm^{-1} spectral regions are assigned to the carbon−carbon single and double bond stretching vibrations, respectively. Those in the 1375−1328 cm^{-1} region and around 1445 cm^{-1} are assigned to the symmetric and asymmetric methyl deformation, respectively. Those in the 1730−1715 cm^{-1} region are assigned to the carbonyl C═O stretchings. In all solutions, the Raman lines of the carbon−carbon double bond stretching vibrations (1550−1530 cm^{-1} spectral region) are the strongest as compared to the other Raman lines. On the basis of the results of resonance Raman spectra, the system origin and the full width at half-maximum (fwhm) of the steady-state absorption spectra were determined by a Franck−Condon analysis as described below.[50]

For transitions from the ground state, $|S_0\rangle$, to the lowest optically allowed excited state, $|S_2\rangle$, with energies $\{E_2\}$, the linear absorption coefficient, $\alpha(\omega)$, defined as the fraction of energy absorbed in passing through an isotropic material, is

$$\alpha(\omega) \propto \sum_l |\langle S_0|\hat{\mu}|S_2\rangle|^2 \cdot F_{lm} \cdot \delta(\omega - \Omega_{02} - l\cdot\omega_v)$$

$F_{lm} = |\langle l|m\rangle|^2$ is a Franck−Condon factor, the square magnitude of the instantaneous overlap of the mth nuclear wave function of the ground state, $|m\rangle$, and the lth nuclear wave function of the excited state, $|l\rangle$. $\hat{\mu}$ is the transition dipole operator for the transition from $|S_0\rangle$ to $|S_2\rangle$. $\Omega_{02} = (E_2 - E_0)/\hbar$ is the angular transition frequency of the state $|S_2\rangle$. ω is the angular frequency of incident light. ω_v is the angular molecular vibrational frequency. Assuming that the steady-state absorption spectra of C20Ind in solution are convoluted with Gaussian sub-bands, we have

$$\alpha(\omega) \propto \sum_l |\langle S_0|\hat{\mu}|S_2\rangle|^2 \cdot F_{lm} \cdot \exp\left(-\frac{(\omega - \Omega_{02} - l\cdot\omega_v)^2}{2\cdot\Gamma^2}\right)$$

$$\Gamma = \frac{\sigma}{2\sqrt{2\ln 2}}$$

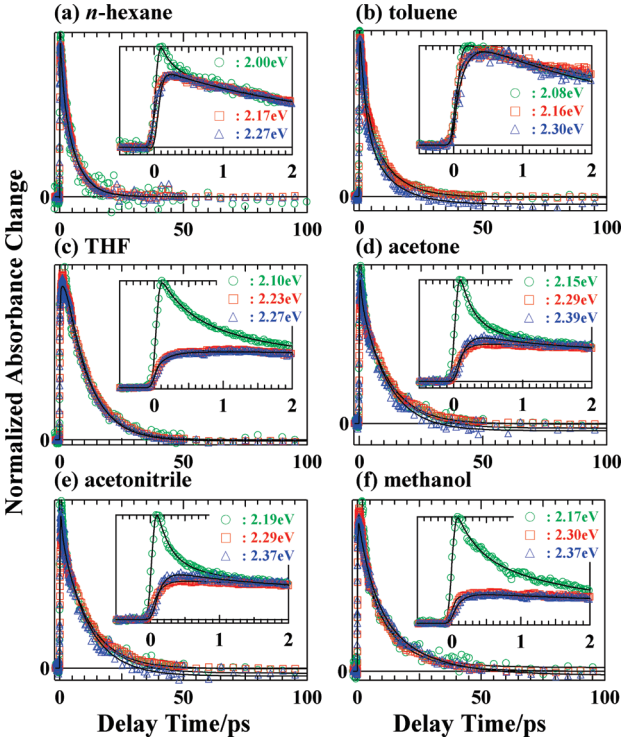

Figure 6. The normalized transient absorption kinetics of C20Ind in (a) *n*-hexane, (b) acetone, (c) THF, (d) acetone, (e) acetonitrile, and (f) methanol. All kinetic traces were normalized using the amplitude at 3 ps after excitation. The "○", "□", and "△" show the experimental data. Solid lines show the results of fitting using multiexponential functions. The insets show the same plots of a short time regime after excitation.

where σ is a full width at half-maximum (fwhm) of a Gaussian function. At the temperature of the system $T = 0$, the lowest vibrational state ($m = 0$) of the ground state is occupied. We define the Franck−Condon factor as

$$F_{l0} = |\langle l|0\rangle|^2 = \frac{S^l \cdot \exp(-S)}{l!}$$

dx.doi.org/10.1021/jp111313f |J. Phys. Chem. A 2011, 115, 2110–2119

Table 2. Solvent Dependence of Decay Time Constants Determined by the Fitting of Transient Absorption Kinetics Following Excitation at 2.43 eV Using Multi-exponential Functions of C20Ind[a]

		time constants			
solvent	probe energy	τ_1/fs	τ_2/ps	τ_3/ps	τ_4/ns
n-hexane	2.00 eV (620 nm)	80 ± 30 (+)	1.3 ± 0.1 (+)	5.6 ± 0.1 (+)	
	2.17 eV (571 nm)	80 ± 30 (−)	1.3 ± 0.1 (+)	5.6 ± 0.1 (+)	
	2.27 eV (546 nm)	80 ± 30 (−)	1.3 ± 0.1 (+)	5.6 ± 0.1 (+)	
toluene	2.08 eV (596 nm)	100 ± 40 (−)	2.6 ± 0.1 (+)	10.7 ± 0.1 (+)	10 (fixed) (−)
	2.16 eV (574 nm)	100 ± 40 (−)	2.6 ± 0.1 (+)	10.7 ± 0.1 (+)	10 (fixed) (−)
	2.30 eV (539 nm)	100 ± 40 (−)	2.6 ± 0.1 (+)	10.7 ± 0.1 (+)	10 (fixed) (−)
THF	2.10 eV (590 nm)	210 ± 60 (+)	1.6 ± 0.4 (+)	9.7 ± 0.2 (+)	
	2.23 eV (556 nm)	210 ± 60 (−)	1.6 ± 0.4 (−)	9.7 ± 0.2 (+)	
	2.27 eV (546 nm)	210 ± 60 (−)	1.6 ± 0.4 (−)	9.7 ± 0.2 (+)	10 (fixed) (−)
acetone	2.15 eV (577 nm)	150 ± 30 (+)	0.82 ± 0.16 (+)	11.2 ± 0.3 (+)	10 (fixed) (−)
	2.29 eV (541 nm)	150 ± 30 (−)	0.82 ± 0.16 (−)	11.2 ± 0.3 (+)	10 (fixed) (−)
	2.39 eV (519 nm)	150 ± 30 (−)	0.82 ± 0.16 (+)	11.2 ± 0.3 (+)	10 (fixed) (−)
acetonitrile	2.19 eV (566 nm)	280 ± 160 (+)	6.4 ± 0.3 (+)	17.5 ± 0.9 (+)	
	2.29 eV (541 nm)	280 ± 160 (−)	6.4 ± 0.3 (+)	17.5 ± 0.9 (+)	
	2.37 eV (523 nm)	280 ± 160 (−)	6.4 ± 0.3 (+)	17.5 ± 0.9 (+)	10 (fixed) (−)
methanol	2.17 eV (571 nm)	200 ± 60 (−)	4.1 ± 0.1 (+)	13.8 ± 0.1 (+)	
	2.30 eV (539 nm)	200 ± 60 (−)	4.1 ± 0.1 (+)	13.8 ± 0.1 (+)	
	2.37 eV (523 nm)	200 ± 60 (−)	4.1 ± 0.1 (+)	13.8 ± 0.1 (+)	10 (fixed) (−)

[a] Plus and minus signs on the right-hand side of decay time constants indicate rise and decay phases, respectively.

where S is a Huang−Rhys factor. Next, we obtain the fitting model function of the steady-state absorption spectra, $A(\omega)$, as

$$A(\omega) \propto \alpha(\omega) \propto \sum_l |\langle S_0|\hat{\mu}|S_2\rangle|^2 \cdot \frac{S^l \cdot \exp(-S)}{l!} \cdot \exp\left(-\frac{(\omega - \Omega_{02} - l\cdot\omega_v)^2}{2\Gamma^2}\right)$$

On the basis of the observed resonance Raman spectra, the frequency of carbon−carbon double bond stretching mode is dominant and hence used as ω_v. S, Ω_{02}, and Γ are determined by spectral fitting.

The calculations (solid lines in Figure 2) agree well with the experimental results. Table 1 summarizes the fitting parameters determined by the Franck−Condon analysis. The large Huang−Rhys factor is due to the large displacement of equilibrium nuclear positions between ground and excited states caused by strong electron−phonon coupling. Figure 4 shows the plots of the 0−0 transition energy and fwhm as a solvent polarity factor, $P_f = (\varepsilon - 1)/(\varepsilon + 2) - (n^2 - 1)/(n^2 + 2)$. This parameter can be derived to combine the Lippert and Mataga equation[51] and the effect of elliptical cavity formed by the surrounding solvent molecules.[52] It is appropriately applicable for the case of carotenoids to explain the solvent-dependent energy shift of optical absorption.[10,52] It is suggested that the system origins of the steady-state absorption spectra are blue-shifted and that the spectral line widths are broadened as solvent polarity increases. This trend is similar to that observed with other carbonyl-containing carotenoids.[4,5,10−13]

Solvent Dependence of Femtosecond Transient Absorption Spectra and Kinetics of C20Ind. Figure 5 shows femtosecond transient absorption spectra of C20Ind in several solvents. In all cases, blue-shifting and narrowing of the transient absorption spectra are observed at early delay times after excitation (0.1, 0.5, and 2 ps). A typical relaxation pathway of carotenoids in nonpolar solvent has been proposed as $S_2 \rightarrow$ hot $S_1 \rightarrow S_1 \rightarrow S_0$.[53−55] On the basis of this idea, the spectral change observed here is assignable to the vibrational relaxation in

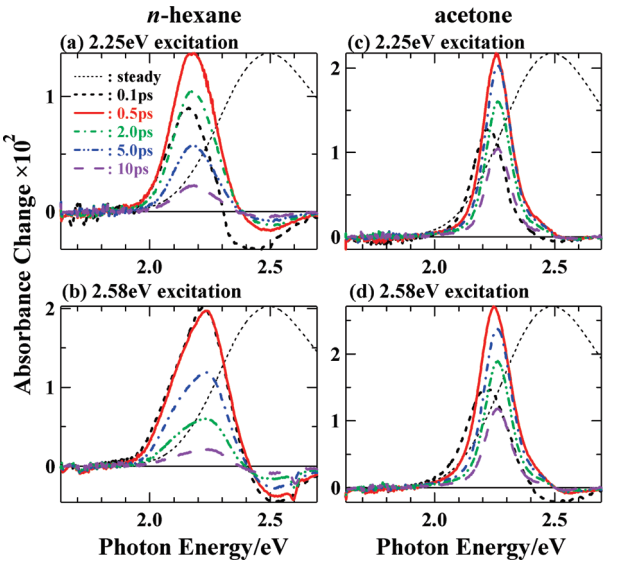

Figure 7. Excitation energy dependence of the transient absorption spectra of C20Ind in *n*-hexane (left-hand side) and acetone (right-hand side). Parts (a) and (b) show the transient absorption spectra in *n*-hexane for 2.25 and 2.58 eV excitaion, respectively. Parts (c) and (d) show those in acetone for 2.25, 2.58 eV excitaion, respectively. Dotted lines show the steady-state absorption spectra. Dashed, solid, dashed−dotted, dashed double-dotted, and long-dashed lines show the femtosecond transient absorption spectra recorded at 0.1, 0.5, 2.0, 5.0, and 10 ps after excitation, respectively.

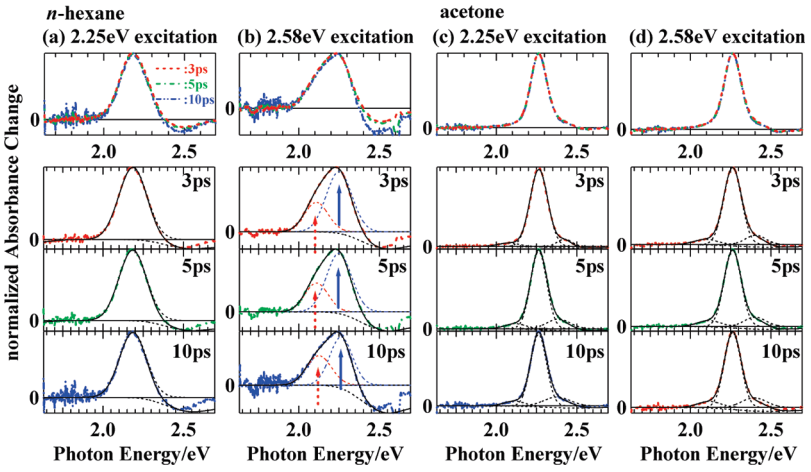

Figure 8. Delay time dependence and spectral decomposition of the normalized transient absorption spectra of C20Ind in *n*-hexane (left-hand side) and acetone (right-hand side). Parts (a) and (b) show the results of spectral decomposition in *n*-hexane following excitation at 2.25 and 2.58 eV, respectively. Parts (c) and (d) show those in acetone following excitation at 2.25 and 2.58 eV, respectively. Dashed, dashed dotted, and dashed double-dotted lines show the femtosecond transient absorption spectra recorded at 3, 5, and 10 ps after excitation, respectively. Solid lines show the results of spectral decomposition determined by two or three Gaussian functions together with the bleaching of the steady-state absorption spectra. Dotted lines show the Gaussian sub-bands determined by the spectral decomposition. Dashed and solid arrows in (b) indicate the lower energy (LE) and the higher energy (HE) bands, respectively.

Table 3. Relative Intensities, Peak Energy, and Full Width at Half-Maximum (fwhm) of Gaussian Profiles of the Excited-State Absorption Components and Relative Bleaching Intensity of the Steady-State Absorption Component Determined by the Convolution of the Transient Absorption Spectra of C20Ind

		lower energy			middle energy			highest energy			
	delay time/ ps	relative intensity	peak energy/ eV	fwhm/ eV	relative intensity	peak energy/ eV	fwhm/ eV	relative intensity	peak energy/ eV	fwhm/ eV	bleaching intensity
2.25 eV excitation	3	1	2.19	0.146	0	/	/	0	/	/	1
in *n*-hexane	5	1	2.18	0.142	0	/	/	0	/	/	0.77
	10	1	2.19	0.139	0	/	/	0	/	/	0.46
2.58 eV excitation	3	0.446	2.11	0.121	1	2.25	0.133	0	/	/	1
in *n*-hexane	5	0.612	2.12	0.128	1	2.26	0.125	0	/	/	0.73
	10	0.656	2.12	0.130	1	2.26	0.119	0	/	/	0.47
2.25 eV excitation	3	0.078	2.11	0.107	1	2.26	0.084	0.183	2.38	0.123	1
in acetone	5	0.083	2.12	0.107	1	2.26	0.083	0.168	2.39	0.114	0.86
	10	0.083	2.11	0.107	1	2.26	0.082	0.152	2.39	0.114	0.51
2.58 eV excitation	3	0.104	2.11	0.121	1	2.26	0.090	0.167	2.40	0.115	1
in acetone	5	0.107	2.11	0.121	1	2.26	0.087	0.157	2.40	0.111	0.86
	10	0.113	2.11	0.121	1	2.26	0.086	0.172	2.40	0.121	0.64

the S_1 state. In the transient absorption spectra in polar solvents (THF, acetone, and acetonitrile) at 5 ps after excitation (dashed double-dotted lines in Figure 5), the peak energy of transient absorption is blue-shifted with an increase of solvent polarity. The spectral band shape does not show significant difference at delay times longer than 2 ps after excitation (Figure 5c−e). A similar trend can be seen in a protic solvent (Figure 5f). In carbonyl-containing carotenoids such as peridinin and fucoxanthin, a transient absorption of the $S_{1\text{-ICT}}$ can be seen at the lower energy side of the $S_1 \rightarrow S_n$ absorption transition band in polar and protic solvents.[4,5,10−13] In Figure 5, however, a new transient absorption band of C20Ind in polar and protic solvents is not detected as compared to that in nonpolar solvents. This phenomenon suggests that the transient absorption of the $S_{1\text{-ICT}}$ state of C20Ind has not been detected. The spectral behavior in nonpolar solvents, however, is quite different from that in polar and protic solvents. The spectral bandwidths of the transient absorption of C20Ind in nonpolar solvents are apparently broader than those in polar solvents. To gain insight into the origin of the spectral broadening, the excitation energy dependence of the transient absorption spectra and their kinetics was investigated, for C20Ind in *n*-hexane and acetone (see next section).

Figure 6 shows the solvent dependence of the transient absorption kinetics of C20Ind. In all cases, the kinetics are well fitted by multiexponential functions. Table 2 summarizes the results of the fitting. Based on the relaxation pathway of typical carotenoids, such as β-carotene, lycopene, zeaxanthin, and spheroidene,[53−55] τ_1, τ_2, and τ_3 correspond to the S_2, hot S_1, and S_1 lifetimes, respectively. 10 ns is regarded as infinity as compared to the time scale in which we are observing the kinetics

dx.doi.org/10.1021/jp111313f |J. Phys. Chem. A 2011, 115, 2110–2119

using femtosecond time-resolved absorption spectroscopy. This value is conventionally adopted and is fixed for the fitting of the kinetics traces. Also, the 10 ns decay component shows good agreement with the bleaching signal of $S_0 \rightarrow S_2$ absorption in the spectral domain. The degradation of C20Ind by direct photoexcitation has already been reported by Fujii et al.[56] Therefore, we assigned the origin of this 10 ns decay component to the bleaching of the $S_0 \rightarrow S_2$ absorption caused by the sample decomposition. The $S_1 \rightarrow S_0$ internal conversion time constant (τ_3 in Table 2) becomes long as solvent polarity increases. This trend is completely opposite to the situation of $S_{1\text{-ICT}}$ dynamics of carbonyl-containing carotenoids, such as peridinin and fucoxanthin.[4,5,10−13] Rather, this trend is reminiscent of the S_1 dynamics of a carotenoid with an aldehyde-type carbonyl group.[29]

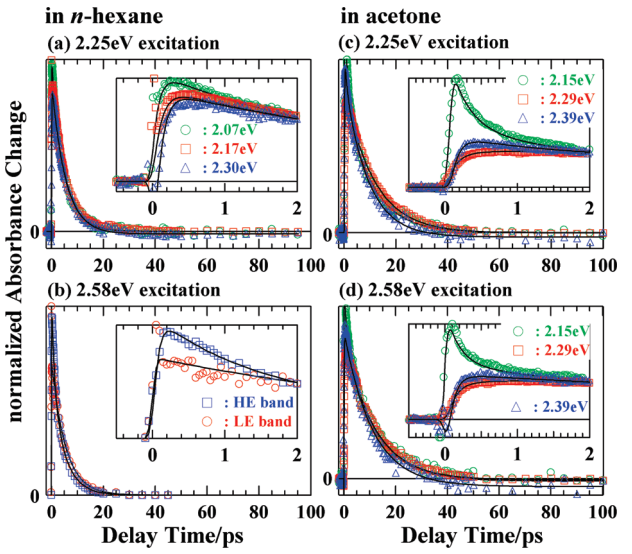

Figure 9. Excitation energy dependence of the kinetics of transient absorbance change of C20Ind (a) in *n*-hexane following excitation at 2.25 eV, (b) in *n*-hexane following excitation at 2.58 eV, (c) in acetone following excitation at 2.25 eV, and (d) in acetone following excitation at 2.58 eV. The "○", "□", and "△" show the experimental data. Solid lines show the results of fitting using multiexponential functions. The insets show the same plots of a short time regime after excitation. "HE band" and "LE band" in (b) correspond to the higher and lower energy subbands, respectively, in Figure 8b.

Excitation Energy Dependence of the Femtosecond Transient Absorption Spectra and Their Kinetics for C20Ind in *n*-Hexane and Acetone. Figure 7 shows the excitation energy dependence of the transient absorption spectra of C20Ind in *n*-hexane and acetone. In all cases, the maxima of transient absorptions show blue shifts between 0.1 and 2 ps. This phenomenon is interpreted as vibronic relaxation in the excited state.[53−55] The transient absorption spectra at longer than 2 ps after excitation in *n*-hexane depend strongly on excitation energy, whereas those in acetone do not. To gain insight into the origin of the spectral difference, spectral decomposition of the transient absorption spectra of C20Ind was carried out.

Figure 8 shows the excitation energy dependence of the normalized transient absorption spectra and the results of the spectral decomposition at delay times after excitation of 3, 5, and 10 ps in both solvents. Table 3 shows the relative intensities, peak energies, and fwhm of the transient absorptions determined by spectral decomposition. In the cases following excitation at 2.25 and 2.58 eV in *n*-hexane, the transient absorption spectra are well reproduced using one or two Gaussian functions together with a bleaching component corresponding to bleaching of the steady-state absorption spectrum, as shown in Figure 8a and b. In the case of both these excitation energies in acetone, three Gaussian functions (the lowest, middle, and the highest energies) and one bleaching component are required to achieve satisfactory fitting of the transient absorption spectra (Figure 8c and d). Transient absorptions following excitation at 2.25 eV in *n*-hexane (Figure 8a) show a similar spectral pattern at each delay time, whereas with those following excitation at 2.58 eV in *n*-hexane the relative intensity of each Gaussian sub-band apparently changes depending on a delay time (see relative intensity of the "lowest energy" and "middle energy" positions following excitation at 2.58 eV in *n*-hexane in Table 3). This suggests that at least two excited states must be involved in the dynamics of these

Table 4. Excitation Energy Dependence of Decay Time Constants Determined by Fitting of Transient Absorption Kinetics of C20Ind Using Multi-exponential Functions[a]

		time constants			
solvent	probe energy	τ_1/fs	τ_2/ps	τ_3/ps	τ_4/ns
		At 2.25 eV (551 nm) Excitation			
n-hexane	2.07 eV (599 nm)	108 ± 17 (−)	1.4 ± 0.1 (+)	5.0 ± 0.1 (+)	
	2.17 eV (571 nm)	108 ± 17 (−)	not applicable	5.0 ± 0.1 (+)	
	2.30 eV (539 nm)	108 ± 17 (−)	not applicable	5.0 ± 0.1 (+)	10 (fixed) (−)
acetone	2.15 eV (577 nm)	110 ± 20 (+)	0.96 ± 0.24 (+)	11.4 ± 0.2 (+)	10 (fixed) (−)
	2.29 eV (541 nm)	110 ± 20 (−)	0.96 ± 0.24 (−)	11.4 ± 0.2 (+)	10 (fixed) (−)
	2.39 eV (519 nm)	110 ± 20 (−)	not applicable	11.4 ± 0.2 (+)	10 (fixed) (−)
		At 2.58 eV (481 nm) Excitation			
n-hexane	LE band	70 ± 100 (−)	not applicable	5.4 ± 0.1 (+)	
	HE band	60 ± 100 (−)	1.1 ± 0.1 (+)	5.0 ± 0.1 (+)	
acetone	2.15 eV (577 nm)	130 ± 40 (+)	0.76 ± 0.10 (+)	10.3 ± 0.4 (+)	
	2.29 eV (541 nm)	130 ± 40 (−)	0.76 ± 0.10 (−)	10.3 ± 0.4 (+)	10 (fixed) (−)
	2.39 eV (519 nm)	130 ± 40 (−)	0.76 ± 0.10 (+)	10.3 ± 0.4 (+)	10 (fixed) (−)

[a] Plus and minus signs on the right-hand side of the decay time constants indicate rise and decay phases, respectively.

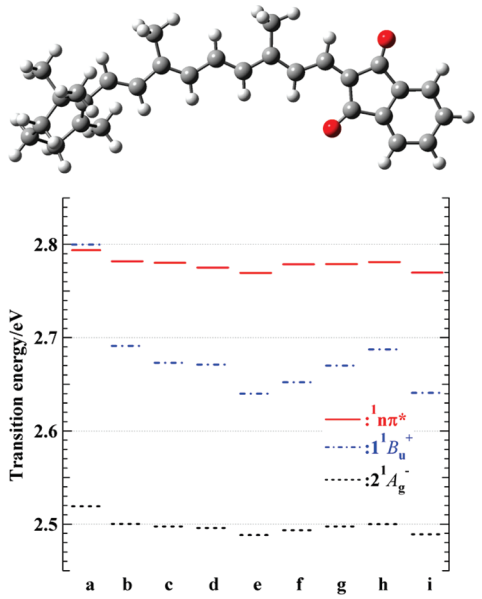

Figure 10. (Top) A ground-state chemical structure of C20Ind determined by density functional B3LYP/6-31G(d) calculation. (Bottom) Energy diagram of three lowest singlet excited states of C20Ind in (a) vacuum, (b) isopentane, (c) cyclohexane, (d) diethyl ether, (e) acetonitrile, (f) benzene, (g) decaline, (h) 3-methylpentane, and (i) ethanol predicted by MNDO-PSDCI calculations. Dotted, dashed, and solid lines show the transition energy of the $2^1A_g^-$, the $1^1B_u^+$, and the $^1n\pi^*$ states of C20Ind, respectively.

transient absorption spectra at times longer than 3 ps after excitation at 2.58 eV.

Transient absorption band shapes in acetone are independent of the delay time and excitation energy. This suggests that the same single excited state was generated following the relaxation from the S_2 state after excitation at 2.25 and 2.58 eV in acetone. Figure 9 shows the excitation energy dependence of the transient absorption kinetics of C20Ind in *n*-hexane and acetone. The sharp peak that appeared instantaneously following excitation has been assigned to nonlinear optical effects.[57,58] In all cases, the kinetics are well fitted by multiexponential functions. Table 4 summarizes the results of this fitting. The lower energy (LE) and higher energy (HE) bands generated following excitation at 2.58 eV in *n*-hexane have different decay time constants (5.4 and 5.0 ps, respectively). Furthermore, the decay time constant of the HE band is close to that of the excited state generated following excitation at 2.25 eV in *n*-hexane. These results suggest that the HE band is the same excited state that is generated following excitation at 2.25 eV. The LE band is generated in a time regime shorter than the instrument response function (~100 fs). Therefore, it can be tentatively concluded that the LE band was generated either by direct photoexcitation or by relaxation from the higher vibrational excited state of the S_2 state. The rise component of the HE band is not synchronous with the decay component of the LE band.

MNDO-PSDCI Calculations of C20Ind. Figure 10 shows the ground-state chemical structure of C20Ind determined by density functional B3LYP/6-31G(d) calculation and the solvent dependence of the energies of the S_2 ($1^1B_u^+$), S_1 ($2^1A_g^-$), and $^1n\pi^*$ states predicted by MNDO-PSDCI calculations. It should be noted that the energies of the S_2 and $^1n\pi^*$ states were determined to be very close (~0.1 eV). Consequently, in the case following excitation at 2.25 eV in *n*-hexane, it is suggested

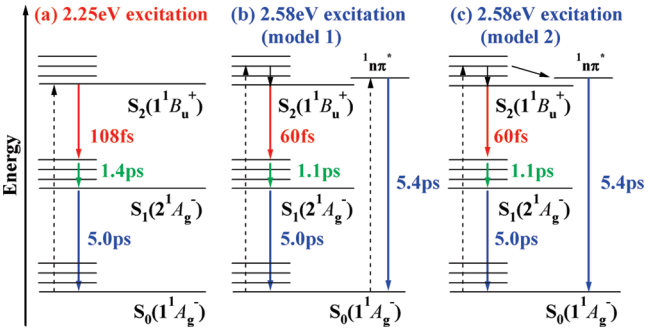

Figure 11. Schematic drawings of the relaxation pathways of C20Ind in *n*-hexane. Dashed arrows show the excitation by incident light. Thin solid arrows indicate the vibrational relaxation in the S_2 or internal conversion from the vibrational excited state of S_2 to the $^1n\pi^*$ state. Thick solid arrows show the relaxation pathways with experimentally determined lifetimes.

that only the S_2 was generated, whereas in the case following excitation at 2.58 eV in *n*-hexane, both the S_2 and the $^1n\pi^*$ states were generated. The S_2 of carotenoids instantaneously relaxes to the S_1.[53−55] Therefore, it is suggested that the HE band produced following excitation at 2.58 eV and the excited state produced following excitation at 2.25 eV in *n*-hexane can be unequivocally assigned to the $S_1 \rightarrow S_n$ transition. The LE band produced following excitation at 2.58 eV in *n*-hexane can then be assigned to the $^1n\pi^*$ state $\rightarrow S_m$ (a higher lying excited state) transition.

Figure 11 shows a schematic description of the relaxation pathways of C20Ind in *n*-hexane based on the experimental results and the calculations. In the case of excitation at 2.25 eV, the relaxation pathway is proposed as $S_2 \rightarrow$ hot $S_1 \rightarrow S_1 \rightarrow S_0$. In the case of excitation at 2.58 eV, two cases are considered for the relaxation pathways of C20Ind. One is that both hot $S_2 \rightarrow S_2 \rightarrow$ hot $S_1 \rightarrow S_1 \rightarrow S_0$ and $^1n\pi^* \rightarrow S_0$ occur simultaneously; the other is that both hot $S_2 \rightarrow S_2 \rightarrow$ hot $S_1 \rightarrow S_1 \rightarrow S_0$ and hot $S_2 \rightarrow {}^1n\pi^* \rightarrow S_0$ occur simultaneously. The latter idea, the branching pathway from the S_2 state, has been reported in previous papers.[59,60] The lifetimes of each excited state of C20Ind were experimentally determined (Table 4). In the previous reports, the $^1n\pi^*$ state was reported to be generated in the relaxation process of the S_1 of retinal having a short polyene chain conjugated with an aldehyde-type carbonyl group.[26−29] On the other hand, it is reported that the nearest underlying state to the S_2 is the $^1n\pi^*$ state for siphonaxanthin, a carbonyl-containing carotenoid with longer conjugated chain length than retinal.[30] The relaxation pathway of siphonaxanthin following excitation to the S_2 is proposed as $S_2 \rightarrow {}^1n\pi^*$ state $\rightarrow S_1 \rightarrow S_0$.[30] The generation and relaxation process of the $^1n\pi^*$ state of C20Ind is clearly different from those of retinal and siphonaxanthin.

On the basis of the calculations, it is expected that both the S_2 and the $^1n\pi^*$ states are generated by the excitation at 2.58 eV in acetone. However, the transient absorption spectra and kinetics are independent of excitation energy, suggesting the production of a single excited state. The lifetime of the $^1n\pi^*$ state of retinal in protic solvents is shorter than that in nonpolar solvents.[29] By inference, on the basis of this observation, it can be suggested that the $^1n\pi^*$ state of C20Ind in acetone is too short-lived to be detected in the present study.

CONCLUSIONS

The steady-state and femtosecond transient absorption spectra of C20Ind in various solvents were investigated. The peak

shift and the broadening of the steady-state absorption spectra with increasing solvent polarity are similar to those observed in other carbonyl-containing carotenoids such as peridinin and fucoxanthin.[4,5,10−13] In contrast, the trend observed for the solvent dependence of the transient absorptions was unusual. The observed solvent dependence was similar to that observed for the S_1 state of retinal.[29] The femtosecond transient absorption spectra of C20Ind following excitation at 2.58 eV in nonpolar *n*-hexane were composed of the two transient absorption bands (the HE and LE bands), whereas in the case of excitation at 2.25 eV only the HE band was observed. The HE and LE bands have been assigned to $S_1 \rightarrow S_n$, and $^1n\pi^*$ states $\rightarrow S_m$ (higher lying excited states), respectively, based on the MNDO-PSDCI calculations. The kinetics of the LE band indicate that the $^1n\pi^*$ state of C20Ind was generated by either direct photoexcitation or relaxation from the higher vibrational excited states of the S_2. The present results suggest that an $S_{1\text{-ICT}}$ does not form in a carotenoid with two carbonyl groups in an *s-cis* conformation relative to the polyene backbone.

AUTHOR INFORMATION

Corresponding Author

*E-mail: hassy@sci.osaka-cu.ac.jp.

ACKNOWLEDGMENT

H.H. thanks the Nissan Science Foundation for financial support. R.J.C. and H.H. thank HFSP for financial support. D.K. was supported in part by the Grant-in-Aid for JSPS Fellows (No. 20002429) from JSPS. The work by H.A.F. was supported by a grant from the National Science Foundation (MCB-0913022) and the University of Connecticut Research Foundation. The work by R.R.B. was supported by the National Institutes of Health (GM-34548) and the National Science Foundation (EMT-0829916).

REFERENCES

(1) Frank, H. A.; Cogdell, R. J. In *Carotenoids in Photosynthesis*; Young, A., Britton, G., Eds.; Chapman and Hall: London, 1993; Chapter 8, pp 252−326.

(2) Frank, H. A.; Cogdell, R. J. *J. Photochem. Photobiol.* **1996**, *63*, 257–264.

(3) Polívka, T.; Sundström, V. *Chem. Rev.* **2004**, *104*, 2021–2071.

(4) Bautista, J. A.; Connors, R. E.; Raju, B. B.; Hiller, R. G.; Sharples, F. P.; Gosztola, D.; Wasielewski, M. R.; Frank, H. A. *J. Phys. Chem. B* **1999**, *103*, 8751–8758.

(5) Frank, H. A.; Bautista, J. A.; Josue, J.; Pendon, Z.; Hiller, R. G.; Sharples, F. P.; Gosztola, D.; Wasielewski, M. R. *J. Phys. Chem. B* **2000**, *104*, 4569–4577.

(6) Zigmantas, D.; Hiller, R. G.; Yartsev, A.; Sundström, V.; Polívka, T. *J. Phys. Chem. B* **2003**, *107*, 5339–5348.

(7) Zigmantas, D.; Hiller, R. G.; Sharples, F. P.; Frank, H. A.; Sundström, V.; Polívka, T. *Phys. Chem. Chem. Phys.* **2004**, *6*, 3009–3016.

(8) Zigmantas, D.; Hiller, R. G.; Sundström, V.; Polívka, T. *Proc. Natl. Acad. Sci. U.S.A.* **2002**, *99*, 16760–16765.

(9) Linden, P. A.; Zimmermann, J.; Brixner, T.; Holt, N. E.; Vaswani, H. M.; Hiller, R. G.; Fleming, G. R. *J. Phys. Chem. B* **2004**, *108*, 10340–10345.

(10) Ehlers, F.; Wild, D. A.; Lenzer, T.; Oum, K. *J. Phys. Chem. A* **2007**, *111*, 2257–2265.

(11) Kopczynski, M.; Ehlers, F.; Lenzer, T.; Oum, K. *J. Phys. Chem. A* **2007**, *111*, 5370–5381.

(12) Wild, D. A.; Winkler, K.; Stalke, S.; Oum, K.; Lenzer, T. *Phys. Chem. Chem. Phys.* **2006**, *8*, 2499–2505.

(13) Niedzwiedzki, D. M.; Chatterjee, N.; Enriquez, M. M.; Kajikawa, T.; Hasegawa, S.; Katsumura, S.; Frank, H. A. *J. Phys. Chem. B* **2009**, *113*, 13604–13612.

(14) Fujii, R.; Inaba, T.; Watanabe, Y.; Koyama, Y.; Zhang, J.-P. *Chem. Phys. Lett.* **2003**, *369*, 165–172.

(15) Kosumi, D.; Fujiwara, M.; Fujii, R.; Cogdell, R. J.; Hashimoto, H.; Yoshizawa, M. *J. Chem. Phys.* **2009**, *130*, 214506−1–214506−8.

(16) Vaswani, H. M.; Hsu, C.-P.; Head-Gordon, M.; Fleming, G. R. *J. Phys. Chem. B* **2003**, *107*, 7940–7946.

(17) Shima, S.; Ilagan, R. P.; Gillespie, N.; Sommer, B. J.; Hiller, R. G.; Sharples, F. P.; Frank, H. A.; Birge, R. R. *J. Phys. Chem. A* **2003**, *107*, 8052–8066.

(18) Premvardhan, L.; Sandberg, D. J.; Fey, H.; Birge, R. R.; Büchel, C.; van Grondelle, R. *J. Phys. Chem. B* **2008**, *112*, 11838–11853.

(19) Kosumi, D.; Kusumoto, T.; Fujii, R.; Sugisaki, M.; Iinuma, Y.; Oka, N.; Takaesu, Y.; Taira, T.; Iha, M.; Frank, H. A.; Hashimoto, H. *Chem. Phys. Lett.* **2009**, *483*, 95–100.

(20) Polívka, T.; Kerfeld, C. A.; Pascher, T.; Sundström, V. *Biochemistry* **2005**, *44*, 3994–4003.

(21) Chábera, P.; Fuciman, M.; Hříbeka, P.; Polívka, T. *Phys. Chem. Chem. Phys.* **2009**, *11*, 8795–8803.

(22) Turro, N. J. *Modern Molecular Photochemistry*; University Science Books: California, 1991; Chapter 5, pp 76−152.

(23) Papanikolas, J.; Walker, G. C.; Sbamamian, V. A.; Christensen, R. L.; Clayton Baum, J. *J. Am. Chem. Soc.* **1990**, *112*, 1912–1920.

(24) Das, P. K.; Becker, R. S. *J. Phys. Chem.* **1982**, *86*, 921–927.

(25) Wardle, B. *Principles and Applications of Photochemistry*; Wiley: New York, 2009; Chapter 1, pp 1−27.

(26) Takeuchi, S.; Tahara, T. *J. Phys. Chem. A* **1997**, *101*, 3052–3060.

(27) Larson, E. J.; Friesen, L. A.; Johnson, C. K. *Chem. Phys. Lett.* **1997**, *265*, 161–168.

(28) Yamaguchi, S.; Hamaguchi, H. *J. Chem. Phys.* **1998**, *109*, 1397–1408.

(29) Yamaguchi, S.; Hamaguchi, H. *J. Phys. Chem. A* **2000**, *104*, 4272–4279.

(30) Akimoto, S.; Yokono, M.; Higuchi, M.; Tomo, T.; Takaichi, S.; Murakami, A.; Mimuro, M. *Photochem. Photobiol. Sci.* **2008**, *7*, 1206–1209.

(31) Hashimoto, H.; Hattori, K.; Okada, Y.; Yoda, T.; Matsushima, R. *Jpn. J. Appl. Phys.* **1998**, *37*, 4609–4615.

(32) Kosumi, D.; Abe, K.; Karasawa, H.; Fujiwara, M.; Cogdell, R. J.; Hashimoto, H.; Yoshizawa, M. *Chem. Phys.* **2010**, *373*, 33–37.

(33) Frisch, M. J.; Trucks, G. W.; Schlegel, H. B.; Scuseria, G. E.; Robb, M. A.; Cheeseman, J. R.; Montgomery, J. A., Jr.; Vreven, T.; Kudin, K. N.; Burant, J. C.; Millam, J. M.; Iyengar, S. S.; Tomasi, J.; Barone, V.; Mennucci, B.; Cossi, M.; Scalmani, G.; Rega, N.; Petersson, G. A.; Nakatsuji, H.; Hada, M.; Ehara, M.; Toyota, K.; Fukuda, R.; Hasegawa, J.; Ishida, M.; Nakajima, T.; Honda, Y.; Kitao, O.; Nakai, H.; Klene, M.; Li, X.; Knox, J. E.; Hratchian, H. P.; Cross, J. B.; Bakken, V.; Adamo, C.; Jaramillo, J.; Gomperts, R.; Stratmann, R. E.; Yazyev, O.; Austin, A. J.; Cammi, R.; Pomelli, C.; Ochterski, J. W.; Ayala, P. Y.; Morokuma, K.; Voth, G. A.; Salvador, P.; Dannenberg, J. J.; Zakrzewski, V. G.; Dapprich, S.; Daniels, A. D.; Strain, M. C.; Farkas, O.; Malick, D. K.; Rabuck, A. D.; Raghavachari, K.; Foresman, J. B.; Ortiz, J. V.; Cui, Q.; Baboul, A. G.; Clifford, S.; Cioslowski, J.; Stefanov, B. B.; Liu, G.; Liashenko, A.; Piskorz, P.; Komaromi, I.; Martin, R. L.; Fox, D. J.; Keith, T.; Al-Laham, M. A.; Peng, C. Y.; Nanayakkara, A.; Challacombe, M.; Gill, P. M. W.; Johnson, B.; Chen, W.; Wong, M. W.; Gonzalez, C.; Pople, J. A. *Gaussian 03*, revision C.02; Gaussian, Inc.: Wallingford, CT, 2004.

(34) Kusumoto, T.; Horibe, T.; Kajikawa, T.; Hasegawa, S.; Iwashita, T.; Cogdell, R. J.; Birge, R. R.; Frank, H. A.; Katsumura, S.; Hashimoto, H. *Chem. Phys.* **2010**, *373*, 71–79.

(35) Martin, C. H.; Birge, R. R. *J. Phys. Chem. A* **1998**, *102*, 852–860.

(36) Hudson, B. S.; Birge, R. R. *J. Phys. Chem. A* **1999**, *103*, 2274–2281.

(37) Kusnetzow, A.; Singh, D. L.; Martin, C. H.; Barani, I.; Birge, R. R. *Biophys. J.* **1999**, *76*, 2370–2389.

(38) Dolan, P. M.; Miller, D.; Cogdell, R. J.; Birge, R. R.; Frank, H. A. *J. Phys. Chem. B* **2001**, *105*, 12134–12142.
(39) Ren, L.; Martin, C. H.; Wise, K. J.; Gillespie, N. B.; Luecke, H.; Lanyi, J. K.; Spudich, J. L.; Birge, R. R. *Biochemistry* **2001**, *40*, 13906–13914.
(40) Kusnetzow, A.; Dukkipati, A.; Babu, K. R.; Singh, D.; Vought, B. W.; Knox, B. E.; Birge, R. R. *Biochemistry* **2001**, *40*, 7832–7844.
(41) Kusnetzow, A. K.; Dukkipati, A.; Babu, K. R.; Ramos, L.; Knox, B. E.; Birge, R. R. *Proc. Natl. Acad. Sci. U.S.A.* **2004**, *101*, 941–946.
(42) Hillebrecht, J. R.; Galan, J.; Rangarajan, R.; Ramos, L.; McCleary, K.; Ward, D. E.; Stuart, J. A.; Birge, R. R. *Biochemistry* **2006**, *45*, 1579–1590.
(43) Rangarajan, R.; Galan, J. F.; Whited, G.; Birge, R. R. *Biochemistry* **2007**, *46*, 12679–12686.
(44) Clark, R. J. H.; D'Urso, N. R.; Zagalsky, P. F. *J. Am. Chem. Soc.* **1980**, *102*, 6693–6698.
(45) Nagae, H.; Kuki, M.; Zhang, J.-P.; Sashima, T.; Mukai, Y.; Koyama, Y. *J. Phys. Chem. A* **2000**, *104*, 4155–4166.
(46) Rimai, L.; Heyde, M. E.; Gill, D. *J. Am. Chem. Soc.* **1973**, *95*, 4493–4501.
(47) Saito, S.; Tasumi, M. *J. Raman Spectrosc.* **1983**, *14*, 310–321.
(48) Koyama, Y.; Fujii, R. In *The Photochemistry of Carotenoids: Applications in Biology*; Frank, H. A., Cogdell, R. J., Young, A. J., Britton, G., Eds.; Kluwer Academic: Dordrecht, 1999; Chapter 9, pp 161−188.
(49) Sigalov, M.; Lemcoff, N. G.; Shainyan, B.; Chipanina, N.; Aksamentova, T. *Eur. J. Org. Chem.* **2010**, *14*, 2800–2811.
(50) Barford, W. *Electronic and Optical Properties of Conjugated Polymers*; Clarendon Press: Oxford, 2005; Chaper 8, pp 113−130.
(51) Shaikh, M.; Mohanty, J.; Singh, P. K.; Bhasikuttan, A. C.; Rajule, R. N.; Satam, V. S.; Bendre, S. R.; Kanetkar, V. R.; Pal, H. *J. Phys. Chem. A* **2010**, *114*, 4507–4519.
(52) Nagae, H.; Kuki, M.; Cogdell, R. J.; Koyama, Y. *J. Chem. Phys.* **1994**, *101*, 6750–6765.
(53) Billsten, H. H.; Zigmantas, D.; Sundström, V.; Polívka, T. *Chem. Phys. Lett.* **2002**, *355*, 465–470.
(54) Cerullo, G.; Lanzani, G.; Zavelani-Rossi, M.; De Silvestri, S. *Phys. Rev. B* **2001**, *63*, 241104-1–241104-4.
(55) Polívka, T.; Zigmantas, D.; Frank, H. A.; Bautista, J. A.; Herek, J. L.; Koyama, Y.; Fujii, R.; Sundström, V. *J. Phys. Chem. B* **2001**, *105*, 1072–1080.
(56) Fujii, R.; Kusumoto, T.; Sashima, T.; Cogdell, R. J.; Gardiner, A. T.; Hashimoto, H. *J. Phys. Chem. A* **2005**, *109*, 11117–11122.
(57) Kosumi, D.; Komukai, M.; Hashimoto, H.; Yoshizawa, M. *Phys. Rev. Lett.* **2005**, *95*, 213601−1–213601−4.
(58) Kosumi, D.; Fujiwara, M.; Hashimoto, H.; Yoshizawa, M. *J. Phys. Soc. Jpn.* **2009**, *78*, 104715−1–104715−5.
(59) Billsten, H. H.; Pan, J.; Sinha, S.; Pascher, T.; Sundström, V.; Polívka, T. *J. Phys. Chem. A* **2005**, *109*, 6852–6859.
(60) Pang, Y.; Fleming, G. R. *Phys. Chem. Chem. Phys.* **2010**, *12*, 6782–6788.